

RESEARCH

Open Access



# Effect of Sand Content on the Workability and Mechanical Properties of Concrete Using Bottom Ash and Dredged Soil-based Artificial Lightweight Aggregates

Kyung-Ho Lee<sup>1</sup>, Keun-Hyeok Yang<sup>2\*</sup> , Ju-Hyun Mun<sup>2</sup> and Nguyen Van Tuan<sup>3</sup>

## Abstract

The objective of this study is to examine the workability and various mechanical properties of concrete using artificial lightweight aggregates produced from expanded bottom ash and dredged soil. Fifteen concrete mixes were classified into three groups with regard to the designed compressive strengths corresponding to 18 MPa, 24 MPa, and 35 MPa. In each group, lightweight fine aggregates were replaced by using natural sand from 0 to 100% at an interval of 25%. Thus, the density of concrete ranged between 1455 and 1860 kg/m<sup>3</sup>. Based on the regression analysis using test data, a reliable model was proposed to clarify lower early-age strength and higher long-term strength gains of lightweight aggregate concrete (LWAC) when compared with the predictions of the *fib* model. The proposed model also indicates that a lower water-to-cement ratio is required with the decrease in the natural sand content to achieve the designed compressive strength of concrete. The partial use natural sand is favorable for enhancing the tensile resistance capacity, shear friction strength, and bond behavior with a reinforcing bar of LWAC. The *fib* model overestimates direct tensile strength, bond strength and the amount of slip at the peak bond stress of LWAC. Therefore, it is necessary to consider the density of concrete as a critical factor in conjunction with its compressive strength to rationally evaluate the various mechanical properties of LWAC.

**Keywords:** lightweight aggregate concrete, density, bottom ash, dredged soil, mechanical properties, sand content, *fib* model

## 1 Introduction

Recently, lightweight aggregates have been artificially produced by the thermal treatment of industrial by-products or waste materials such as fly ash, bottom ash, palm oil fuel ash, and dredged soil (Aslam et al. 2016; Jo et al. 2007; Lotfy et al. 2015; Yang et al. 2011). It is commonly known that these types of recycled artificial lightweight aggregates are structurally strong, physically stable, durable, and environmentally favorable (Jo et al. 2007). The internal void structure, stiffness, strength, and substrate

characteristics of the artificial lightweight aggregates are dependent on the chemical composition and fineness of the source materials (Chandra and Berntsson 2003), and this eventually influences the interaction between the paste matrix and lightweight aggregate particles. Thus, crack propagation and tensile resistance capacity of concrete using artificial lightweight aggregates fluctuates with the chemical composition and physical quality of the source materials used producing the artificial aggregate particles. This implies that it is necessary to examine the reliability of code equations for mechanical properties of lightweight aggregate concrete (LWAC) when different types and qualities of source materials are selected for producing artificial lightweight aggregates.

The workability and mechanical properties of LWAC significantly depend on the grading and physical

\*Correspondence: yangkh@kgu.ac.kr

<sup>2</sup> Department of Architectural Engineering, Kyonggi University, Suwon, Kyonggi-do, South Korea

Full list of author information is available at the end of the article

Journal information: ISSN 1976-0485 / eISSN 2234-1315

properties of aggregate particles (Chandra and Berntsson 2003). The lightweight aggregates typically possess higher water absorption and lower density when compared with those of the conventional normal-weight aggregates. High water absorption by the aggregates leads to rapid slump loss and shorter setting time of fresh concrete when the aggregates are not pre-controlled by moist treatment prior to mixing (Yang et al. 2014). The rapid setting time also results in high shrinkage of concrete at an early age. Aggregate particles with a lower density when compared with that of the surrounding cementitious matrix may cause segregation since they flow to the upper surface of the concrete. Furthermore, artificial lightweight aggregates frequently exhibit discontinuous particle distribution and especially in the case of fine aggregates due to the difficulty of producing a particle size less than 1.25–2.5 mm. The discontinuous grading of the aggregate particles reduces the tensile resistance capacity of concrete that leads to the development of unexpected cracks in concrete members.

Structural LWAC is commonly defined (ACI Committee 211 1998; ACI Committee 213 2014; ACI Committee 318 2014; Comité Euro-International du Béton 2010) as concrete that is composed of lightweight aggregate conforming to ASTM C 330 (2012) and that satisfies the requirements of a 28-day compressive strength exceeding 17 MPa and air-dried density ( $\gamma_{ca}$ ) of 1600–1840 kg/m<sup>3</sup>. Based on  $\gamma_{ca}$  and the 28-day compressive strength ( $f'_c$ ) of concrete, ACI 211 (1998) classifies concrete into two types, namely all-LWAC ( $\gamma_{ca} < 1760$  kg/m<sup>3</sup> and  $f'_c > 17$  MPa) and sand-LWAC ( $\gamma_{ca} < 1840$  kg/m<sup>3</sup> and  $f'_c > 17$  MPa). The *fib* model code (2010) categorizes the LWAC into eight types based on oven-dried density ( $\gamma_c$ ) and  $f'_c$ , thereby indicating that the compressive strength of LWAC is closely related with its density. To enhance the workability and compressive strength of LWAC, the fine lightweight aggregates are often partially or fully replaced by using natural sand although the combination with natural sand increases  $\gamma_c$ . The combination with natural sand is also a better solution to improve the grading of fine lightweight aggregates. However, extant studies indicate the absence of available test data (Lv et al. 2015; Shafiqh et al. 2014) to examine the effect of the partial addition of natural sand on the workability and mechanical properties of LWAC. Shafiqh et al. (2014) indicated that the use of oil palm shell for replacing natural sand up to 50% can potentially produce structural LWAC, although the decreasing rate of the  $\gamma_c$  of this type of concrete is insignificant when compared with the  $\gamma_c$  of concrete in which 100% natural sand is used. Yang et al. (2014) also mentioned that the field applications of concrete fabricated by using lightweight aggregate particles with discontinuous grade are typically difficult because

it is not easy to determine the mixing proportions necessary to achieve the designed concrete due to segregation. Hence, there is paucity of understanding related to the reliability and safety estimations of code equations for the mechanical properties of LWAC based on the combination ratios of natural sand and fine lightweight aggregates.

In the early 2010s, the commercial production of the recycled artificial lightweight aggregates using the combination of bottom ash and dredged soil was promoted in Korea. The present study prepared 15 concrete mixtures to examine the effect of the natural sand content on the workability and mechanical properties of concrete using Korean artificial lightweight aggregates. Slump, air content, and segregation was measured in the fresh concrete. With respect to the hardened concrete, the following mechanical properties were tested: compressive strength development, direct tensile strength ( $f_t$ ), splitting tensile strength ( $f_{sp}$ ), stress–strain relationship, moduli of elasticity ( $E_c$ ) and rupture ( $f_r$ ), shear friction strength ( $\tau_f$ ), and bond stress–slip relationship of a reinforcing bar embedded into the concrete. Based on the nonlinear regression analysis using test data, compressive strength development equation including 28-day strength was formulated as a function of  $\gamma_c$  and water-to-cement ratio ( $W/C$ ). The various measured mechanical properties measured in the present LWAC specimens were compared (wherever possible) with the predictions obtained from the design equations recommended in the *fib* model code (Comité Euro-International du Béton 2010). The measured moduli of elasticity and rupture were also compared with the predictions obtained from ACI 318-14 equations (2014).

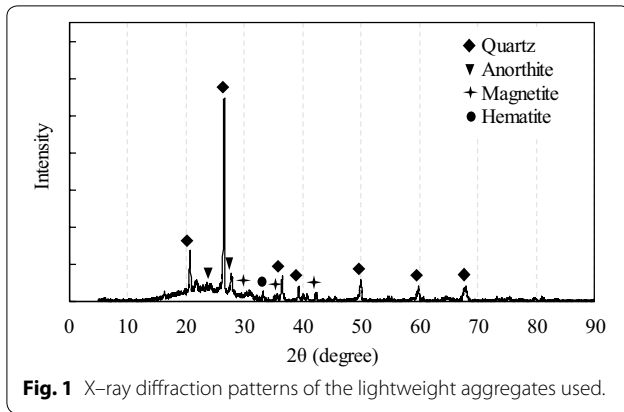
## 2 Significance of Research

This study provides comprehensive test data to examine the different mechanical properties of lightweight concrete using artificially expanded bottom ash and dredged soil granules (hereafter, this concrete type is referred to as LWAC-BS). Test results ascertained that the density of concrete should be considered as a critical factor in conjunction with its compressive strength to evaluate the various mechanical properties of LWAC-BS. In addition, the reliable design equations for compressive strength development of LWAC-BS are proposed on the basis of the regression analysis using test data. Overall, this study confirmed that the code equations for mechanical properties of LWAC-BS need to improve their validity.

## 3 Experimental Details

### 3.1 Materials

Ordinary Portland cement conforming to ASTM Type 1 (2012) was used as a basic cementitious material for all



the mixes. Artificially expanded granules that are commercially available in Korea were used for structural lightweight aggregates. The bottom ash and dredged soil used for the source materials of the lightweight granules are calcined and expanded in large rotary kilns at approximately 1200 °C. The main compositions of the lightweight aggregates measured from X-ray diffraction included quartz and calcium aluminum silicate (Fig. 1), that are close to the compositions commonly observed in the source materials. The maximum particle sizes of lightweight coarse and fine aggregates were 19 mm and 4.75 mm, respectively. Locally available natural sand with a maximum size of 1.2 mm was also used for the replacement ( $R_s$ ) of the lightweight fine aggregates to control the

discontinuous grading of the lightweight fine aggregates. The lightweight aggregates were spherical in shape and exhibited a dense surface structure with a slightly smooth texture, as shown in Fig. 2. The core of the particle exhibited a uniformly fine and porous structure, that enabled weight lightening although it induced a high absorption in conjunction with low strength and stiffness.

The physical properties of the aggregates used are summarized in Table 1. The apparent density and water absorption were 1.0 g/cm<sup>3</sup> and 17.2%, respectively, for lightweight coarse particles, and 1.1 g/cm<sup>3</sup> and 12.9%, respectively, for lightweight fine particles. The quality of the artificially expanded granules satisfies the requirements for structural lightweight aggregates specified in ASTM C330 (2012). The apparent density and water absorption of coarse aggregates were slightly lower when compared with those of the lightweight fine aggregates. The water absorption of lightweight aggregates was excessively high whereas their apparent density was approximately 35% lower when compared with that of natural sand. The particle distribution of lightweight fine aggregates indicated discontinuous grading without any particle interference, thereby indicating ‘gap-grading’ (Collins and Sanjayan 1999b), as shown in Fig. 3. Particles less than 1.25 mm in size were almost undetected in the lightweight aggregates. Thus, they are inconsistent with the standard distribution curves recommended in the ASTM C330 (2012). The fineness modulus of lightweight fine aggregates and sand were 4.4 and 2.2, respectively.

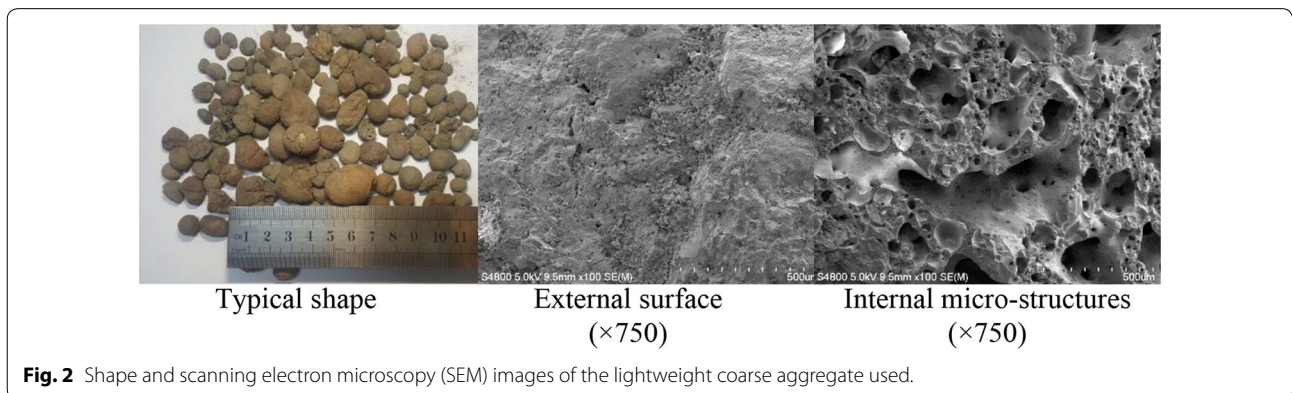


**Table 1** Properties of the aggregates used.

Type		Maximum size (mm)	Specific gravity	Water absorption (%)	Fineness modulus
Coarse aggregate	Expanded granules	19.00	1.0	17.2	6.4
Fine aggregate	Expanded granules	4.75	1.1	12.9	4.4
	Sand	1.20	1.7	1.6	2.2

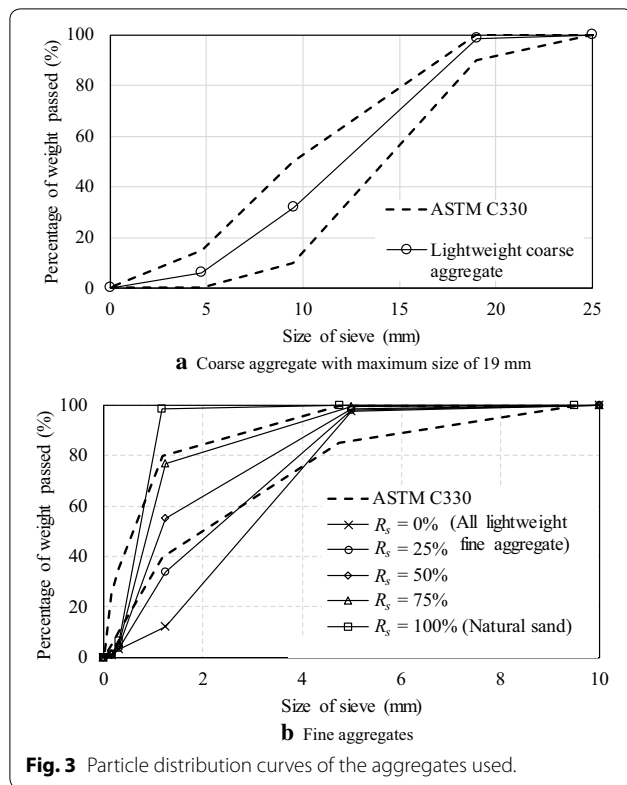


**Fig. 3** Particle distribution curves of the aggregates used.

On the other hand, the particles combined by using lightweight fine aggregates and sand exhibited continuous grading, which nearly satisfied the standard distribution

curves of the ASTM C330 (2012). The fineness modulus of the combined fine aggregates tended to decrease when the content of natural sand increased. The lightweight coarse aggregates also satisfied the standard distribution curves, thereby indicating a fineness modulus of 6.4.

### 3.2 Concrete Mixtures

Fifteen concrete mixes were prepared and classified into three groups based on the following designed compressive strength ( $f_{cd}$ ): L-group for  $f_{cd}$  of 18 MPa, M-group for  $f_{cd}$  of 24 MPa, and H-group for  $f_{cd}$  of 35 MPa. In each group, lightweight fine aggregates were replaced by using the natural sand from 0 to 100% at an interval of 25%, as shown in Table 2. Thus, the specimen notation includes two parts. The first part identifies the compressive strength group of concrete and the other part refers to  $R_s$ . For example, specimen L-25 indicates a lightweight concrete mixture proportioned using 25% sand ( $R_s = 25\%$ ) and 75% lightweight fine aggregates to achieve  $f_{cd}$  of 18 MPa. Mixtures of L-0, M-0, and H-0 indicate all-lightweight concrete without natural sand, and the other mixtures are categorized into sand-lightweight concrete. The mixture proportions of all the concrete specimens were determined based on the procedure proposed by Yang et al. (2014). In all the mixes, the initial slump value exceeding 150 mm was targeted for considering a smooth casting. Thus, the  $W/C$  varied at a fixed fine aggregate-to-total aggregate ratio of 40% in all the mixtures to achieve  $f_{cd}$ . Even the  $W/C$  in each group slightly decreased with decreases in  $R_s$ , indicating that a lower

**Table 2** Mixture proportions of the concrete specimens.

Specimens	Replacement level using sand, $R_s$ (%)	W/C (%)	Unit weight (kg/m <sup>3</sup> )				
			Cement	Water	Lightweight fine aggregate	Natural sand	Lightweight coarse aggregate
L-0	0	52.0	319	185	400	0	560
L-25	25	53.5	327	185	302	171	563
L-50	50	55.1	336	185	202	343	566
L-75	75	56.6	346	185	101	517	568
L-100	100	58.0	356	185	0	692	570
M-0	0	47.0	330	185	393	0	550
M-25	25	48.5	339	185	296	168	553
M-50	50	50.1	350	175	204	346	570
M-75	75	51.6	382	175	102	522	573
M-100	100	53.0	394	175	0	699	576
H-0	0	35.0	415	170	384	0	538
H-25	25	36.5	430	170	291	165	543
H-50	50	38.0	447	170	196	333	549
H-75	75	39.5	466	170	99	504	553
H-100	100	40.9	486	170	0	676	557

$W/C$  is required for concrete with increase in the lightweight fine aggregate content at the same  $f_{cd}$ . Moreover, a higher  $f_{cd}$  required a lower  $W/C$ .

### 3.3 Casting, Curing, and Testing

Lightweight aggregates and natural sand were prepared in the saturated surface dried (SSD) state that is commonly employed in ready-mixed concrete plants. In order to simulate the SSD state, all aggregates were damped for 24 h and subsequently air-dried for another 24 h in outdoor shade. Immediately prior to mixing, the moisture content in aggregates was measured and subsequently accounted for the calculation of the net unit water content of each mixture proportion to avoid excessive bleeding or segregation of fresh concrete due to the high absorption of lightweight aggregates. For all concrete mixes, a water-reducing agent was not added. The initial slump and air content of fresh concrete were measured in accordance with ASTM C143 (2012) and ASTM C231 (2012), respectively. After testing the initial slump, standard molds were cast to measure various mechanical properties of hardened concrete. All specimens were consolidated in accordance with the casting requirements by vibration specified in ASTM C31 (2012) and then cured in a room temperature until they were tested at the specified age. All steel molds were removed at an age of 3 days. In order to examine the segregation or floating of lightweight aggregates, digital image analysis was conducted on the longitudinally cut  $100 \times 200$  mm cylinders. The dark gray contrast indicated expanded lightweight particles and was profiled through an image analysis of all quarter zones of the cutting plane. The area of the aggregate particles in each quarter zone was recorded from the image analysis to calculate the share portion of each component.

The various mechanical properties of hardened concrete were measured as follows: compressive strength gain with age,  $f_t$ ,  $f_{sp}$ ,  $E_c$ ,  $f_r$ ,  $\tau_f$ , stress–strain relationship, and bond stress–slip relationship of a reinforcing bar embedded into the concrete. The compressive strength of concrete was recorded by using  $100 \times 200$  mm cylinder specimens at ages corresponding to 3, 7, 28, 56, and 91 days. The stress–strain curve and modulus of elasticity were recorded at the age of 28 days, whereas the other mechanical properties were measured at 91 days because of a large number of specimens. The air-dried and oven-dried densities of the concrete was recorded at the age of 28 days based on the procedure outlined in ASTM C138 (2012). In order to obtain the stress–strain curve and calculate  $E_c$  at the 40% of peak stress (ASTM C469 2012), a compressor meter with built-in 10 mm capacity dial gages and electrical resistance strain gages (ERS) was mounted on the cylinder specimens. To evaluate

the tensile resistance capacity of concrete,  $f_t$ ,  $f_{sp}$ , and  $f_r$  were measured. Splitting tensile tests were conducted using  $100 \times 200$  mm cylinder specimens in accordance with ASTM C469 (2012). The modulus of rupture was obtained from beam tests conducted in accordance with ASTM C78 (2012). The direct tensile tests were prepared referring the approach proposed by Choi et al. (2014). The dimensions of the I-shaped tensile specimen were  $250 \times 150 \times 100$  mm at both ends with embedded studs and  $100 \times 100 \times 100$  mm at the test zone in the web of a specimen. To minimize tensile eccentricity, the tension load was applied based on RILEM recommendations (1994). The shear friction strength of the concrete specimens was recorded by push-off tests (Yang et al. 2012b) under a concentric load acting as pure shear in the shear plane of the test zone. The push-off specimens had width, height, depth, and critical shear plane area of 300 mm, 800 mm, 120 mm, and  $200 \times 120$  mm, respectively. The bond stress–slip response between concrete and a reinforcing steel bar was estimated by a pullout test using a 150 mm cube incorporated with a 16 mm diameter deformed bar with a yield strength of 600 MPa. The amount of slip was measured at the free end of the reinforcing bar embedded into concrete using a dial gage with 5 mm capacity (Yang et al. 2012a).

## 4 Test Results and Discussions

### 4.1 Initial Slump and Air Content

All the mixtures with the exception of specimens H-0 and H-25 exhibited high slump values exceeding 200 mm, as shown in Table 3, although a water-reduced agent was not added. This implies that the relatively round and smooth surface texture of the lightweight aggregate particles is favorable for improving the initial workability of concrete. The initial slump of LWAC-BS tended to decrease when  $R_s$  decreased. This trend increasingly significant for H-group mixtures. The slump of concrete with  $R_s$  of 0% (all-lightweight concrete) was lower by 9% for the L-Group and 26% for the H-Group when compared with those of the concrete with  $R_s$  corresponding to 100%. In order to satisfy the designed compressive strength, a slightly lower  $W/C$  was applied in each group when  $R_s$  decreases, which resulted in a decrease in the initial slump.

The air content of LWAC-BS was insignificantly affected by  $R_s$  and  $W/C$ , as shown in Table 3. The air content ranged between 4.0 and 6.0% and satisfied the requirements recommended for an air-entrained LWAC that is not exposed to freezing (ACI Committee 213 2014). The LWAC exhibited a higher air content when compared with the conventional normal-weight concrete (NWC) without any air-entraining agent.

**Table 3 Summary of the test results.**

Specimens	Air content (%)	Slump (mm)	Density, $\gamma_c$ (kg/m <sup>3</sup> )	Compressive strength (MPa)					Modulus of elasticity (MPa)	Tensile resistance			Shear friction strength		Bond strength					
				Air-dried	Oven-dried	3 d	7 d	28 d		56 d	91 d	$f_t$ (MPa)	$\frac{f_t}{\sqrt{f'_c(91)}}$	$f_{sp}$ (MPa)	$\frac{f_{sp}}{\sqrt{f'_c(91)}}$	$f_r$ (MPa)	$\frac{f_r}{\sqrt{f'_c(91)}}$	$\tau_f$ (MPa)	$\frac{\tau_f}{\sqrt{f'_c(91)}}$	$\tau_b$ (MPa)
L-0	5.8	230	1502	1301	10.3	13.1	20.8	23.4	27.5	11,728	1.32	0.25	2.21	0.42	3.35	0.64	3.15	0.60	6.37	1.40
L-25	4.0	250	1631	1409	10.0	13.0	18.9	22.1	26.2	13,007	1.46	0.29	2.24	0.44	3.39	0.66	3.23	0.63	6.62	1.52
L-50	5.0	245	1676	1486	9.8	12.5	18.2	22.4	25.4	13,288	1.48	0.29	2.25	0.45	3.49	0.69	3.41	0.68	6.65	1.56
L-75	4.0	255	1758	1528	9.4	11.7	17.6	21.6	24.8	14,184	1.75	0.35	2.28	0.46	3.52	0.71	3.87	0.78	7.10	1.69
L-100	6.2	250	1758	1540	8.8	11.0	17.1	21.1	23.5	14,091	1.86	0.38	2.35	0.48	3.59	0.74	4.01	0.83	7.27	1.76
M-0	4.5	235	1455	1366	15.6	23.0	26.7	30.3	34.1	11,200	1.65	0.28	2.24	0.38	4.22	0.72	3.22	0.55	6.01	1.16
M-25	4.9	210	1557	1491	15.4	20.2	25.8	28.8	33.4	13,152	1.74	0.30	2.28	0.39	4.39	0.76	3.66	0.63	6.25	1.23
M-50	4.3	230	1649	1611	14.9	19.6	24.8	28.0	33.0	14,227	1.84	0.32	2.31	0.40	4.48	0.78	3.80	0.66	6.89	1.38
M-75	4.6	245	1694	1641	13.9	18.8	24.8	28.0	32.4	14,901	1.87	0.33	2.34	0.41	4.50	0.79	3.87	0.68	7.13	1.43
M-100	4.6	240	1753	1698	13.8	17.7	23.0	27.3	32.1	15,259	1.91	0.34	2.44	0.43	4.70	0.83	4.12	0.73	7.45	1.55
H-0	4.8	165	1675	1605	29.1	36.1	38.9	43.6	46.3	16,981	1.88	0.28	2.80	0.41	4.18	0.61	3.60	0.53	7.97	1.28
H-25	4.8	175	1722	1667	28.5	35.3	36.7	43.0	45.8	17,299	1.98	0.29	2.85	0.42	4.43	0.66	4.09	0.60	8.13	1.34
H-50	5.1	210	1755	1686	27.1	34.2	35.8	42.6	44.8	17,752	2.07	0.31	3.36	0.50	4.67	0.70	4.12	0.62	8.10	1.35
H-75	4.8	215	1788	1757	26.8	33.2	35.3	42.2	43.8	18,200	2.17	0.33	3.66	0.55	4.95	0.75	4.41	0.67	8.22	1.38
H-100	5.0	225	1860	1783	25.9	33.1	35.1	41.3	43.6	19,374	2.01	0.30	3.70	0.56	5.06	0.77	4.65	0.70	8.37	1.41

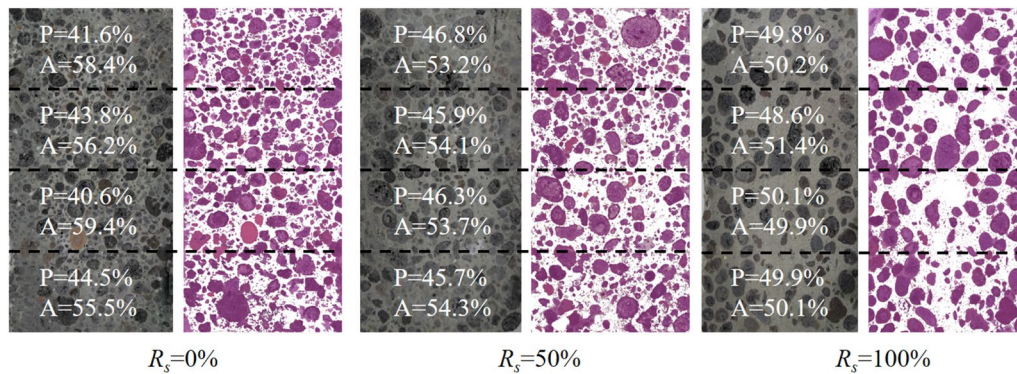


**Fig. 4** Distribution of lightweight aggregate particles with respect to the height of cylinder specimens in the L-group (Note: P and A indicate the cement matrix including natural sand and lightweight granules, respectively).

### 4.2 Segregation

Problems were not specifically encountered in terms of the mixing duration. Figure 4 presents the typical distribution of lightweight aggregate particles relative to the height of a 100 × 200 mm cylinder consolidated by the vibration method in the L-group. Distinct segregation or floating of lightweight aggregate particles was not observed in all specimens. A similar share of lightweight aggregate particles was obtained in each quarter zone of a specimen irrespective of  $R_s$ . The difference in the share of lightweight aggregate particles between the top and bottom quarter zones corresponded to a maximum of 3%.

### 4.3 Compressive Strength at 28 Days

Most of the concrete mixes achieved the  $f_{cd}$  at an age of 28 days, although specimens L-75, L-100, and M-100 exhibited a slightly lower strength when compared with the designed value, as shown in Table 3. The 28 day-compressive strength ( $f'_c$ ) of concrete was insignificantly affected by  $R_s$  because a lower  $W/C$  was selected when  $R_s$  decreased (i.e., with the increase in the content of fine lightweight aggregate). The  $f'_c$  of all-lightweight concrete (with  $R_s=0\%$ ) was only 10.8–21.6% higher than that of the companion concrete with  $R_s=100\%$  because a  $W/C$  that was approximately 6% lower was applied for the former mixes when compared with that for the latter ones. The cracks inducing failure planes of LWAC generally pass through the lightweight aggregates and the number of interfacial cracks between lightweight aggregates and cement matrix increases with the increase in the lightweight aggregate content (Sim et al. 2013). Thus, the increased content of lightweight aggregates mixed in the concrete leads to a lower compressive strength of concrete. Thus, a lower  $W/C$  is required with the decrease in  $R_s$  to achieve the designed compressive strength of concrete.

Generally, the compressive strength of concrete is considered as inversely proportional to  $W/C$  and air content ( $v_A$ ) (Bogas and Gomes 2013; Yang et al. 2014). An increase in the content of natural sand increases  $\gamma_c$ , as shown in Table 3. Thus, the increase in  $R_s$  indicates the increase in  $\gamma_c$ . Given the demand for a lower  $W/C$  with the decrease in  $R_s$  to achieve a targeted compressive strength,  $\gamma_c$  should be considered as a critical factors along with  $W/C$  and  $v_A$  that influences the compressive strength of LWAC. Yang et al. (2014) empirically formulated the simple equation for  $f'_c$  based on an optimum non-linear multiple regression (NLMR) analysis of these influencing parameters using an extensive database that included 39 all-lightweight concrete mixes and 308 sand-lightweight concrete mixes. Figure 5 shows the comparisons of measured  $f'_c$  and predictions obtained from the equation proposed by Yang et al. (2014). The best-fit curve determined from the present test data yielded a higher  $f'_c$  when compared with that of Yang et al.'s equation. Specifically, the grading and substrate of lightweight aggregate particles are factors that influenc  $f'_c$  of LWAC

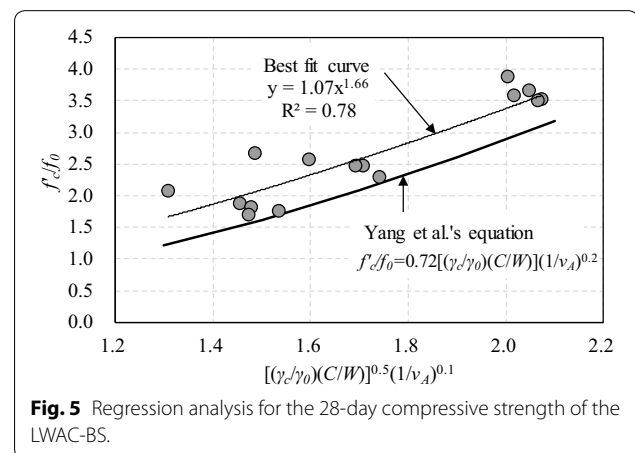


**Fig. 5** Regression analysis for the 28-day compressive strength of the LWAC-BS.

to a certain degree because crack propagation and localized crack zone in the concrete under concentric axial load are affected by the strength of each ingredient of concrete and cohesive capacity between aggregates and cement matrix (Sim et al. 2013). Thus, to reasonably predict the  $f'_c$  of LWAC-BS, the equation proposed by Yang et al. needs to be revised as follows:

$$\frac{f'_c}{f_0} = 1.07 \cdot \left( \frac{\gamma_c}{\gamma_0} \cdot \frac{C}{W} \right)^{0.83} \left( \frac{1}{v_A} \right)^{0.17} \quad (1)$$

where  $f_0$  (= 10 MPa) is the reference value for the 28-day compressive strength of concrete, and  $\gamma_0$  (= 2300 kg/m<sup>3</sup>) is the reference value for the oven-dry density of concrete.

#### 4.4 Compressive Strength Development

Figure 6 shows the typical compressive strength gain of LWAC-BS with respect to the age. The compressive strength ( $f'_c(t)$ ) at different ages is normalized by  $f'_c$  of the corresponding specimen. The compressive strength development of LWAC-BS occurred in a parabolic shape, thereby indicating that the increasing rate of compressive strength gradually decreased with age. The strength gain ratio at 3-day relative to the 28-day strength was generally less than 0.52 for L-group concrete, 0.59 for M-group concrete, and 0.76 for H-group concrete. The strength gain ratio up to an age of 7 days was insignificantly affected by  $R_s$  although it tended to increase with the decrease in  $W/C$ . The strength gain ratio in the long-term was lower for the H-group specimens when compared with that for the L-group specimens. The average values of the strength gain ratio at 91-day relative to the 28-day strength were 1.38 for L-group concrete, 1.32 for M-group concrete, and 1.23 for H-group concrete. The long-term strength gain ratios are higher when compared with the conventional values of 1.05–1.2 determined from NWC (ACI Committee 318). As noted by Collins and Sanjayan (1999a),

lightweight aggregates with high water absorption favorably affect the long-term strength development owing to the continuous hydration caused by the moisture released from the saturated aggregates. This phenomenon was increasingly evident in LWAC-BS with higher  $W/C$ .

In a manner similar to the parabolic strength gain curve of NWC, *fib* mode (2010) proposes the following exponential equation to properly estimate the compressive strength of LWAC-BS at different ages:

$$f'_c(t) = \exp \left\{ S_l \cdot \left[ 1 - \left( \frac{28}{t} \right)^{0.5} \right] \right\} \cdot f'_c \quad (2)$$

where  $t$  is the concrete age in days and  $S_l$  is a coefficient that depends on the strength of the lightweight aggregate. The value of  $S_l$  is identified as 0.05 for lightweight aggregates of high strength and 0.25 for lightweight aggregates of low strength although an explicit comment on the strength classification of lightweight aggregates is not provided. Additionally, the *fib* model does not consider the variation in the strength gain ratio of concrete based on the mixing proportions of LWAC. However, the slopes at the ascending and descending branches of the parabolic strength gain curve depend on  $W/C$  and  $R_s$  (or  $\gamma_c$ ), as discussed in the previous section. Thus,  $S_l$  as defined in the *fib* model does not yield a result consistent with the test result, as shown in the comparisons (Fig. 6) between experiments and predictions. The predictions by *fib* model tend to overestimate the early strength gain whereas it underestimates the long-term strength gain. These inconsistent estimations are increasingly prominent when the  $S_l$  value of 0.05 is employed in Eq. (2) based on the assumption of high-strength lightweight aggregates.

With respect to the reliable estimation of compressive strength of LWAC-BS at different ages, the values of  $S_l$  in each concrete specimen were determined based on the regression analysis using test results. Based on the numerous adjustments of the influencing parameters on  $S_l$  using test data, optimum NLMR analysis results were obtained, as shown in Fig. 7. Overall, the coefficient  $S_l$  in Eq. (2) can be expressed for LWAC-BS using the expanded bottom ash and dredged soil granules as follows:

$$S_l = \left( \frac{W}{C} \right)^{1.98} \left( \frac{\gamma_c}{\gamma_0} \right)^{-0.63} \quad (3)$$

#### 4.5 Stress–Strain Relationship

Typical stress–strain curves measured from the concrete specimens are plotted in Fig. 8. In the same figure, predictions obtained using the model proposed by the *fib* model code are presented for comparison purposes. In contrast to the ACI 318-14 provision (2014), the *fib*

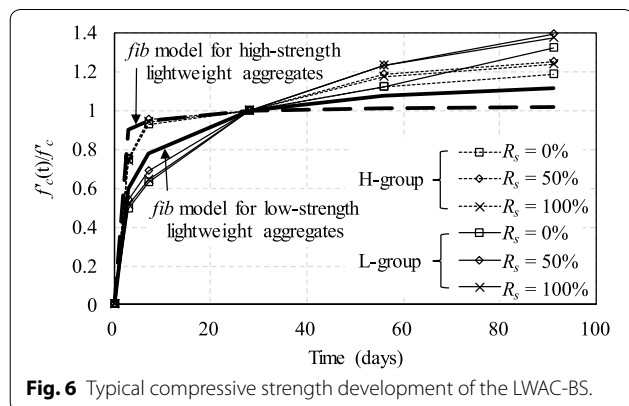
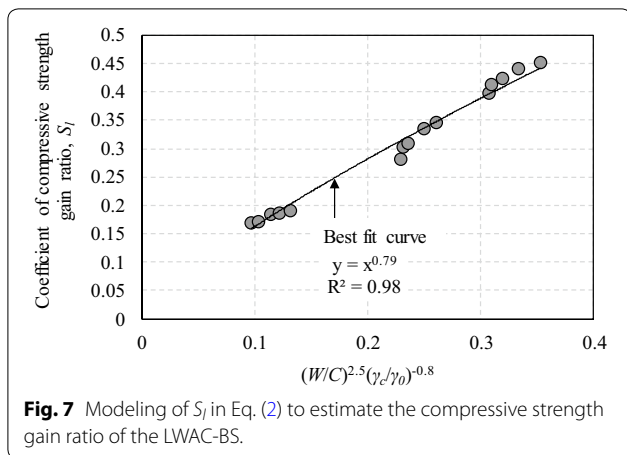
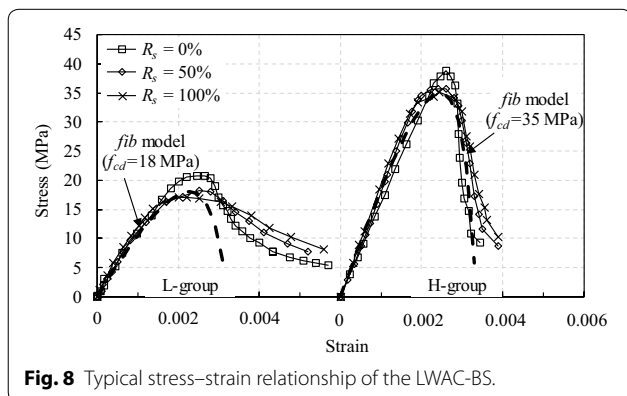


Fig. 6 Typical compressive strength development of the LWAC-BS.



**Fig. 7** Modeling of  $S_f$  in Eq. (2) to estimate the compressive strength gain ratio of the LWAC-BS.

model code (2010) considers lower stiffness and crack resistance capacities of LWAC in terms of mechanical properties including stress–strain relationship and tensile resistance. The shape of a compressive stress–strain curve of LWAC is characterized as a parabola with its vertex at the peak stress. With the decrease in  $R_s$  (or decrease in  $\gamma_c$ ), the slope at the ascending branch decreased whereas the descending branch after peak stress indicated a more rapid decrease. The strains at the peak stress also increased with the decrease in  $R_s$ . Additionally, the decreasing rate of the stresses at the descending branch was greater for concrete with higher  $f'_c$ . Overall, the characteristics of the stress–strain relationship of LWAC are significantly dependent on  $f'_c$  and  $\gamma_c$ . The *fib* model code determines the shape of stress–strain curve of concrete as a function of plasticity number that refers to the ratio of the initial modulus and the secant modulus from the origin to the peak stress. To determine the secant modulus, the effect of lightweight fine aggregates on the strain at the peak stress is considered using experimental constants including 1.1 for lightweight sand and 1.3 for natural sand. This implies



**Fig. 8** Typical stress–strain relationship of the LWAC-BS.

that the *fib* model code does not provide a rational approach to determine the effect of  $\gamma_c$  on the shape of stress–strain curve of concrete. It should be noted that the predictions shown in Fig. 8 are obtained using the constant of 1.2 as a linear interpolation between lightweight fine aggregate and natural sand to calculate the strain at the peak stress. The predictions obtained from equations specified in *fib* model exhibit a more rapid decrease in stresses at the descending branch when compared with the measured curves for the L-group concrete. Furthermore, the *fib* model tends to slightly underestimate the strains at the peak stress irrespective of  $f'_c$ . The inconsistency in the observation between experiments and predictions was increasingly significant for the concrete with lower  $f'_c$ .

### 5 Modulus of Elasticity ( $E_c$ )

As shown in Table 3,  $E_c$  tended to decrease with decreases in  $f'_c$  and  $\gamma_c$ . Figure 9 shows a comparison of the measured  $E_c$  and the predictions calculated from the design equations of the ACI 318-14 and *fib* model. The normalized modulus of elasticity ( $E_c/\sqrt{f'_c}$ ) increased with the increase in  $\gamma_c$ . Hence, the code equations consider a lower increasing rate in  $E_c$  than in  $f'_c$  by using a power function of  $f'_c$ . Both code equations exhibit extremely close values of the  $E_c/\sqrt{f'_c}$  at the same  $\gamma_c$  and indicate consistent agreement with the measurements of the present LWAC-BS specimens. The increasing rate of  $E_c/\sqrt{f'_c}$  with respect to  $\gamma_c$  also corresponds closely in the test results and predictions by code equations.

#### 5.1 Tensile Resistance Capacity

In order to evaluate the tensile resistance capacity of LWAC, the normalized direct tensile strength ( $f_t/\sqrt{f'_c(91)}$ ), normalized splitting tensile strength ( $f_{sp}/\sqrt{f'_c(91)}$ ), and normalized modulus of rupture

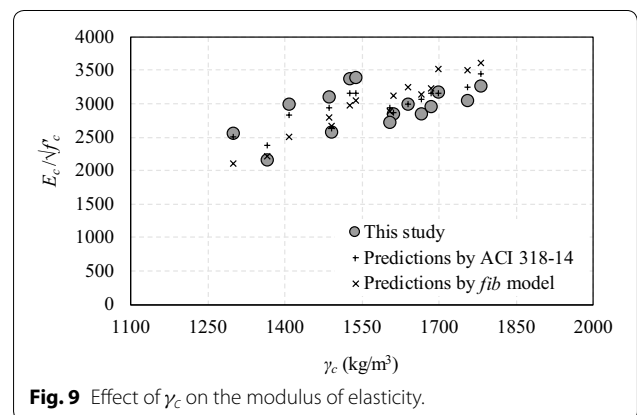


**Fig. 9** Effect of  $\gamma_c$  on the modulus of elasticity.

$(f_r/\sqrt{f'_c(91)})$  are shown in Table 3 and Fig. 10. In the same figure, predictions by the design equations specified in *fib* model are also plotted. It should be noted that the tensile resistance capacity is normalized by using the compressive strength measured at the same age. It is difficult to conduct the direct tensile tests of concrete, and thus the *fib* model recommends the use of conversion factors to determine the direct tensile strength from the splitting tensile strength and the modulus of rupture. The normalized tensile resistance of LWAC-BS tended to increase slightly with the increase in  $\gamma_c$  (or with the increase in  $R_s$ ) irrespective of the concrete compressive strength. For example, concrete with  $R_s=100\%$  exhibits a higher value by 15.6%, 15.3%, and 26.2% for L-, M-, and H-groups, respectively, when compared with the value of  $f_r/\sqrt{f'_c(91)}$  measured in concrete with  $R_s=0\%$ . This implies that the replacement of lightweight fine aggregates using natural sand is favorable for enhancing the tensile resistance capacity of LWAC, given that discontinuous grading of lightweight fine aggregates deteriorates the tensile resistance capacity of concrete due to the increase of the internal voids between particles. The values of  $f_t/\sqrt{f'_c(91)}$ ,  $f_{sp}/\sqrt{f'_c(91)}$ , and  $f_r/\sqrt{f'_c(91)}$  range between 0.25 and 0.38, 0.42 and 0.48, and 0.64 and 0.74, respectively, for L-group specimens, between 0.28 and 0.34, 0.38 and 0.43, and 0.72 and 0.83, respectively, for M-group, and between 0.28 and 0.30, 0.41 and 0.56, and 0.61 and 0.77, respectively, for H-group. Overall, the normalized tensile capacities were insignificantly affected by the concrete compressive strength.

When compared with the predictions obtained by using the *fib* model equation, a close agreement is observed for the modulus of rupture and splitting tensile strength, whereas the model overestimates the direct tensile strength. The mean values of the ratios

between experimental and predicted values were 0.70, 1.0, and 0.97 for the direct tensile strength, splitting tensile strength, and modulus of rupture, respectively. The *fib* model code assumes that LWAC possesses the same strength in both direct tensile and splitting tensile resistances although 20% higher splitting tensile strength is allowed for NWC. Table 3 reveals that the splitting tensile strength of LWAC-BS is higher by 26–68% for L-group, 24–35% for M-group, and 44–86% for H-group, when compared with the direct tensile strength measured in the companion specimen. This implies that the difference between splitting and direct tensile strengths is higher for LWAC-BS when compared with for NWC. Figure 10 also shows that the modulus of rupture of LWAC is conservatively estimated by using the design equation of ACI 318-14, indicating that the mean values of the ratios between experimental and predicted values are 1.39 for L-group, 1.57 for M-group, and 1.40 for H-group.

### 5.2 Shear Friction Strength

The normalized shear friction strength ( $\tau_f/\sqrt{f'_c(91)}$ ) exhibited a tendency to slightly increase with the increase in  $\gamma_c$  (or the increase in  $R_s$ ), as shown in Fig. 11. The value of  $\tau_f/\sqrt{f'_c(91)}$  measured in LWAC-BS with  $R_s=100\%$  was higher by 38.3% for L-group, 32.7% for M-group, and 32.1% for H-group specimens when compared with those of the companion LWAC with  $R_s=0\%$ . The increasing rate of  $\tau_f/\sqrt{f'_c(91)}$  relative to the increase in  $\gamma_c$  was independent of the concrete compressive strength. The frictional failure of a concrete member under pure shear is critically governed by the magnitude of primary tensile stress along shear cracking planes (Yang and Ashour 2015). Thus, the shear and tensile capacities of concrete are indispensable for each other, indicating that the rupture of aggregate particles due to crack propagation

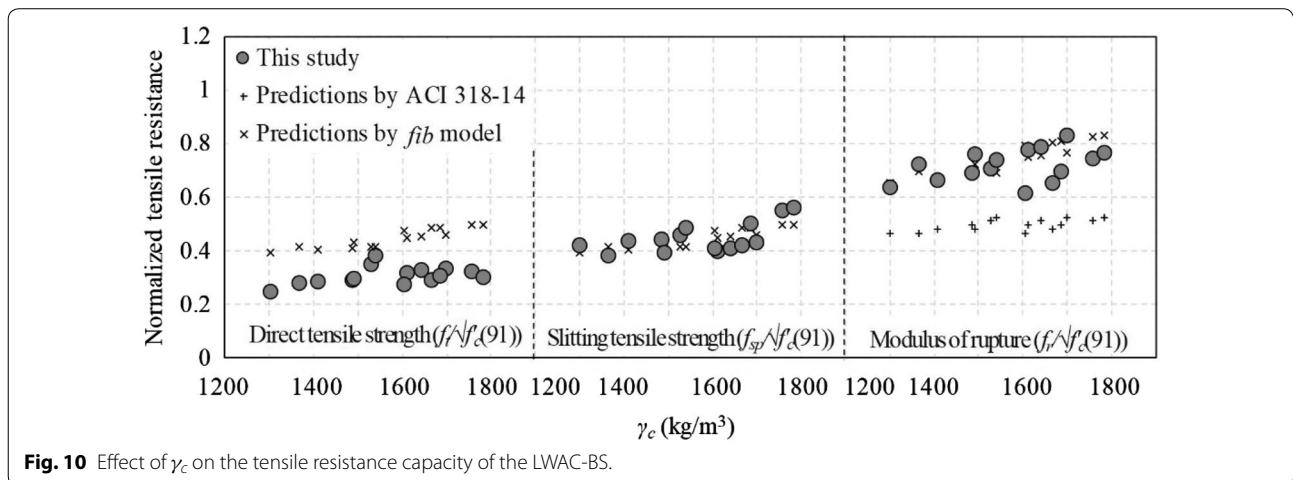
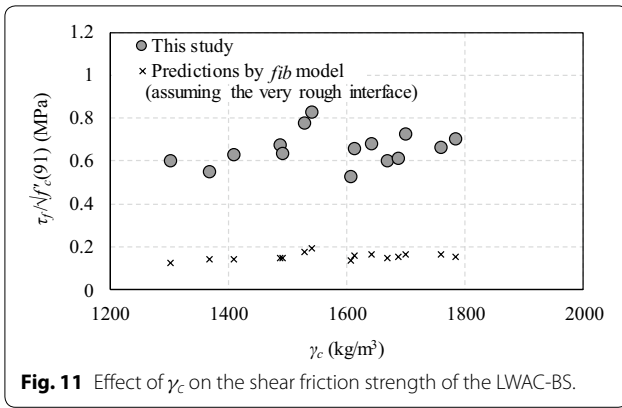
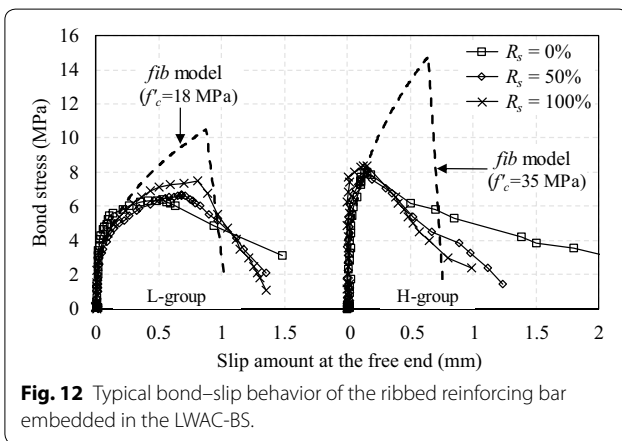


Fig. 10 Effect of  $\gamma_c$  on the tensile resistance capacity of the LWAC-BS.



**Fig. 11** Effect of  $\gamma_c$  on the shear friction strength of the LWAC-BS.



**Fig. 12** Typical bond-slip behavior of the ribbed reinforcing bar embedded in the LWAC-BS.

results in a reduction in the coefficient of friction of concrete. Therefore, it is extremely important to consider the modification factor in evaluating the shear friction strength of concrete. The *fib* model code considers that the shear friction at the interface without reinforcement is entirely resisted by adhesion and aggregate interlock. However, the model code does not specify the adhesive bond for the monolithic interface. The results are considerably underestimated if a coefficient for the adhesive bond resistance along an extremely rough interface, such as shear keys, is employed for the present specimens.

### 5.3 Bond Stress–Slip Response

The typical bond stress–slip relationship of a ribbed steel reinforcing bar embedded into the concrete specimens is plotted in Fig. 12. In the same figure, the predictions determined by using the *fib* model are plotted under a good bond condition for unconfined concrete. The amount of slip at the ascending branch of the bond stress–bar slip curve was insignificantly affected by  $R_s$ , whereas a lower slip was observed for concrete specimens with higher compressive strength. Thus, the slip amount at the peak stress was considerably lower for the H-group

when compared with that for the L-group concrete. After the peak state, the bond stress sharply decreased with the splitting failure of concrete. The decreasing rate of the bond stresses at the descending branch was independent of  $R_s$  and compressive strength of concrete. Meanwhile, the bond strength tended to increase with the increase in  $R_s$  irrespective of compressive strength of concrete. The value of the normalized bond strength ( $\tau_b / \sqrt{f'_c(91)}$ ) measured in LWAC-BS with  $R_s=100\%$  was higher by 25.7% for L-group, 33.6% for M-group, and 10.1% for H-group specimens when compared with those of the companion LWAC-BS with  $R_s=0\%$ . The *fib* model overestimates the amount of slip at the peak stress and bond strength of LWAC-BS. This overestimation is increasingly prominent with the increase in  $f'_c$ . The mean values of the ratios between experimental and predicted bond strengths are 0.59 for L-group, 0.55 for M-group, and 0.62 for H-group specimens. The *fib* model does not consider the effect of the content and physical properties of the lightweight aggregate on the slip resistance of a bar embedded into concrete. The *fib* model code mentions that the coefficient of variation of the bond stress–bar slip response as high as 30% is frequently observed in a laboratory test. However, a reasonable model would be necessary to account for the characteristics of slip resistance of the LWAC-BS.

## 6 Conclusions

This study examined the effect of natural sand content and water-to-cement ratio on the mechanical properties of lightweight aggregate concrete using expanded bottom ash and dredged soil granules (LWAC-BS). The results indicate that the density of concrete should be considered as a critical factor in conjunction with its compressive strength to evaluate the various mechanical properties of LWAC-BS. Based on the increasingly reliable test results, it would be also necessary to establish comprehensible design equations for the mechanical properties of LWAC-BS. From the experimental results and comparisons with code equations, the following conclusions can be drawn:

1. The strength gain ratio up to an age of 7 days was insignificantly affected by the natural sand content ( $R_s$ ) for replacing lightweight fine aggregates; however, the long-term strength gain ratio was higher when compared with the conventional values of 1.05–1.2 as determined from normal-weight concrete.
2. With the decrease in  $R_s$ , the slope at the ascending branch of the stress–strain curve decreased whereas the descending branch after peak stress exhibited a

more rapid decrease. This observation was increasingly evident for concrete with a higher compressive strength.

- The normalized tensile resistance capacity of LWAC-BS tended to increase slightly with the increase in  $R_s$  irrespective of compressive strength of concrete, indicating that using natural sand as the replacement of lightweight fine aggregates is favorable for enhancing the tensile resistance capacity of LWAC.
- The normalized shear friction strength ( $\tau_f/\sqrt{f'_c(91)}$ ) exhibited a tendency to slightly increase with the increase in  $R_s$ , indicating that the increasing rate of  $\tau_f/\sqrt{f'_c(91)}$  was independent of the compressive strength of concrete.
- The amount of slip at the ascending branch of the bond stress–bar slip curve was insignificantly affected by  $R_s$ , whereas a lower slip was observed for concrete specimens with a higher compressive strength. Additionally, the bond strength tended to increase with the increase in  $R_s$  irrespective of the compressive strength of concrete.
- The predictions obtained from the design equations of the *fib* model are in good agreement with the test results for the moduli of elasticity and rupture and splitting tensile strength, whereas the *fib* model overestimates the compressive strength gain at an early age, direct tensile strength, bond strength and the amount of slip at the peak bond stress of the LWAC-BS.

#### Abbreviations

ERS: Electrical resistance strain; LWAC: Lightweight aggregate concrete; LWAC-BS: Lightweight aggregate concrete using expanded bottom ash and dredged soil granules; NLMR: Non-linear multiple regression; NWC: Normal-weight concrete; SSD: Saturated surface dried.

#### Authors' contributions

All authors contributed to this research with respect to the followings: the first and second authors designed the present experimental program and conducted testing; the second author analysed test data and prepared this manuscript; the third author reviewed the previous relevant researches and code provisions; and the fourth author reviewed the overall manuscript and took part in discussion to improve the quality of the research. All authors read and approved the final manuscript.

#### Author details

<sup>1</sup> Department of Architectural Engineering, Kyonggi University Graduate School, Seoul, South Korea. <sup>2</sup> Department of Architectural Engineering, Kyonggi University, Suwon, Kyonggi-do, South Korea. <sup>3</sup> Department of Building Materials, National University of Civil Engineering, Hanoi, Vietnam.

#### Acknowledgements

This work was supported by the National Research Foundation of Korea (NRF) grant funded by the Korea Government (MSIP) (No. NRF-2017R1A2B3008463).

#### Competing interests

The authors declare that they have no competing interests.

#### Availability of data and materials

Not applicable.

#### Consent for publication

Not applicable.

#### Ethics approval and consent to participate

Not applicable.

#### Funding

Not applicable.

#### Publisher's Note

Springer Nature remains neutral with regard to jurisdictional claims in published maps and institutional affiliations.

Received: 11 April 2018 Accepted: 27 September 2018

Published online: 29 January 2019

#### References

- ACI Committee 211. (1998). *Standard practice for selecting proportions for structural lightweight concrete (ACI 211.2-98)*. American Concrete Institute.
- ACI Committee 213. (2014). *Guide for structural lightweight-aggregate concrete (ACI 213R-14)*. American Concrete Institute.
- ACI Committee 318. (2014). *Building code requirements for structural concrete (ACI 318-14)*. Farmington Hills, MI: American Concrete Institute.
- Aslam, M., Shafiq, P., & Jumaat, M. Z. (2016). Oil-palm by-products as lightweight aggregate in concrete mixture-A review. *Journal of Cleaner Production*, 126(2016), 56–73.
- ASTM C31, C78 C138, C143, C231, C330, C469. (2012). *Annual book of ASTM standards: V. 4.02*. ASTM International.
- Bogas, J. A., & Gomes, A. (2013). A simple mix design method for structural lightweight aggregate. *Materials and Structures*, 46(11), 1919–1932.
- Chandra, S., & Berntsson, L. (2003). *Lightweight aggregate concrete: science, technology and applications*. USA: Noyes Publications.
- Choi, S. J., Yang, K. H., Sim, J. I., & Choi, B. J. (2014). Direct tensile strength of lightweight concrete with different specimen depths and aggregate sizes. *Construction and Building Materials*, 63(2014), 132–141.
- Collins, F., & Sanjayan, J. G. (1999a). Strength and shrinkage properties of alkali-activated slag concrete containing porous coarse aggregate. *Cement and Concrete Research*, 29(4), 607–610.
- Collins, F. G., & Sanjayan, J. G. (1999b). Workability and mechanical properties of alkali activated slag concrete. *Cement and Concrete Research*, 29(3), 455–458.
- Comité Euro-International du Béton. (2010). *fib Model Code for Concrete Structures 2010*. International Federation for Structural Concrete (*fib*).
- Jo, B. W., Park, S. K., & Park, J. B. (2007). Properties of concrete made with alkali-activated fly ash lightweight aggregate (AFLA). *Cement and Concrete Composites*, 29(2), 128–135.
- Lotfy, A., Hossain, K. M. A., & Lachemi, M. (2015). Lightweight self-consolidating concrete with expanded shale aggregate: modeling and optimization. *International Journal of Concrete Structure and Materials*, 9(2), 185–206.
- Lv, J., Zhou, T., Du, Q., & Wu, H. (2015). Effects of rubber particles on mechanical properties of lightweight aggregate concrete. *Construction and Building Materials*, 91(2015), 145–149.
- RILEM. (1994). *CPC7: Direct tension of concrete specimens 1975 TC14-CPC*. RILEM technical Recommendations for the testing and use of construction materials.
- Shafiq, P., Mahmud, H. B., Jumaat, M. Z. B., Ahmmad, R., & Bahri, S. (2014). Structural lightweight aggregate concrete using two types of waste from the palm oil industry as aggregate. *Journal of Cleaner Production*, 80(2014), 187–196.
- Sim, J. I., Yang, K. H., Kim, H. Y., & Choi, B. J. (2013). Size and shape effects on compressive strength of lightweight concrete. *Construction and Building Materials*, 38(2013), 854–864.
- Yang, K. H., & Ashour, A. F. (2015). Modification factor for lightweight concrete beams. *ACI Structural Journal*, 112(4), 485–492.

- Yang, K. H., Cho, A. R., & Song, J. K. (2012a). Effect of water–binder ratio on the mechanical properties of calcium hydroxide-based alkali-activated slag concrete. *Construction and Building Materials*, 29(2012), 504–511.
- Yang, K. H., Kim, G. H., & Choi, Y. H. (2014). An initial trial mixture proportioning procedure for structural lightweight aggregate concrete. *Construction and Building Materials*, 55(2014), 431–439.
- Yang, K. H., Mun, J. H., Lee, K. S., & Song, J. K. (2011). Test on cementless alkali-activated slag concrete using lightweight aggregates. *International Journal of Concrete Structure and Materials*, 5(2), 125–131.
- Yang, K. H., Sim, J. I., Kang, J. H., & Ashour, A. F. (2012b). Shear capacity of monolithic concrete joints without transverse reinforcement. *Magazine of Concrete Research*, 64(9), 767–779.

**Submit your manuscript to a SpringerOpen<sup>®</sup> journal and benefit from:**

- ▶ Convenient online submission
- ▶ Rigorous peer review
- ▶ Open access: articles freely available online
- ▶ High visibility within the field
- ▶ Retaining the copyright to your article

---

Submit your next manuscript at ▶ [springeropen.com](https://www.springeropen.com)

---